

The \tilde{X}^1A_1 , \tilde{a}^3B_1 and \tilde{A}^1B_1 Electronic States of the Aluminum Dihydride Anion

Brian C. Hoffman, Yukio Yamaguchi, and Henry F. Schaefer III*

Center for Computational Quantum Chemistry, University of Georgia, Athens, Georgia 30602

Received: December 10, 1998

The three lowest-lying electronic states of the aluminum dihydride anion (AlH_2^-) were systematically investigated using ab initio electronic structure theory. Self-consistent-field (SCF), two-configuration self-consistent-field (TCSCF), complete active space self-consistent-field (CASSCF), configuration interaction including single and double excitations (CISD), and CASSCF-based second-order configuration interaction (SOC) levels of theory were employed with five basis sets of triple- ζ quality. All three electronic states were predicted to possess bent equilibrium geometries. Total electronic energies as well as physical properties including dipole moments, harmonic vibrational frequencies, and associated infrared (IR) intensities were determined for each state. At the CISD level with the largest basis set employed, triple- ζ plus triple polarization augmented with two sets of higher angular momentum functions and two sets of diffuse functions [TZ3P-(2f,2d)+2diff], the equilibrium geometries of the three states were predicted to be $r_e = 1.681$ Å and $\theta_e = 95.6^\circ$ (\tilde{X}^1A_1), $r_e = 1.617$ Å and $\theta_e = 117.8^\circ$ (\tilde{a}^3B_1), and $r_e = 1.594$ Å and $\theta_e = 118.7^\circ$ (\tilde{A}^1B_1). At the same level of theory, the dipole moments with respect to the center of mass were predicted to be 0.64 (\tilde{X}^1A_1), 0.03 (\tilde{a}^3B_1), and 0.24 D (\tilde{A}^1B_1). The energy separations (T_0) between the ground (\tilde{X}^1A_1) and first two excited states predicted at the CASSCF-SOCI level with the TZ3P(2f,2d)+2diff basis set were 14.1 ($\tilde{a}^3B_1 \leftarrow \tilde{X}^1A_1$) and 29.0 kcal mol $^{-1}$ ($\tilde{A}^1B_1 \leftarrow \tilde{X}^1A_1$).

I. Introduction

The AlH_2^- anion is isovalent with methylene, a molecule which, due to past controversies between theory and experiment,^{1–3} has become the benchmark around which many high-level ab initio methods were developed. Theoretical predictions for methylene have attained an accuracy comparable to experiment^{4–11} with relative energy splittings between electronic states approaching 0.1 kcal mol $^{-1}$ accuracy.^{6,10–14} The success of high-level ab initio methods on methylene suggested that predictions of a similar quality could be attained for species isoelectronic (NH_2^+ , H_2O^{++}) or isovalent to methylene (SiH_2 , GeH_2 , PH_2^+ , and AlH_2^-). In particular, those molecules containing heavier atoms such as Al, Si, and P would benefit greatly from such a reliable theoretical study due to the difficulty of obtaining experimental data. Theoretical predictions currently exist for the SiH_2 ¹⁵ and PH_2^+ ¹⁶ molecules, both of which contain second-row atoms and should share several characteristics with AlH_2^- , including a multitude of low-lying electronic states. The existence of these low-lying electronic states suggest that for AlH_2^- there may be one or more excited states below the electron detachment threshold, predicted at 1.15 eV (26.5 kcal mol $^{-1}$) using G2 theory.¹⁷

To date, relatively little information, either experimental or theoretical, exists in the literature for the AlH_2^- anion. In addition to the adiabatic electron affinity of neutral AlH_2 , i.e., the adiabatic electron detachment energy of the anion recently reported by Mayer and Radom,¹⁷ the AlH_2^- anion was investigated by Cramer, Dulles, Storer, and Worthington as part of a systematic investigation of 1A_1 – 3B_1 singlet–triplet gaps in first-, second-, and third-row dihydrides which are isoelectronic/isovalent to methylene.¹⁸ They optimized the 1A_1 and 3B_1 electronic states of AlH_2^- at the full-valence complete active space self-consistent-field (CASSCF) level with an aug-cc-pVTZ basis modified by excising the f functions (Mod-aug-ccpVTZ)

and at two density functional levels with a “TZ2P” basis set. Their best T_e value for the singlet–triplet gap, -13.7 kcal mol $^{-1}$ (the negative sign indicating that the 1A_1 state resides lower in energy than the 3B_1 state), was determined using an “estimated” MRCISD(Q) including all single and double excitations out of the CASSCF references and the Langhoff–Davidson (Q) correction for quadruple excitations. The inclusion of a zero-point vibrational energy (ZPVE) correction increased the predicted gap by 0.6 kcal mol $^{-1}$, yielding their final reported T_0 value of -14.3 kcal mol $^{-1}$.

The goal of this research is to expand upon the results reported by Cramer et al. and to systematically predict, with basis sets including up to three sets of polarization functions and two sets of diffuse and higher angular momentum functions, the relative energy separations and physical properties including dipole moments, harmonic vibrational frequencies, and associated IR intensities for the three lowest electronic states of AlH_2^- . Results obtained for AlH_2^- will be compared to those previously obtained for SiH_2 ¹⁵ and PH_2^+ ¹⁶ with an emphasis on identifying trends. Finally, the energy of the first two excited states, relative to the adiabatic detachment energy of the extra electron, will be reported.

II. Electronic Structure Considerations

Prior results on other second-row hydrides isovalent with methylene, PH_2^+ and SiH_2 , indicated a preference for a closed-shell 1A_1 electronic ground state with a bent equilibrium geometry. Following the same trend, AlH_2^- has a 1A_1 ground state which may be qualitatively expressed as

$$[\text{core}](4a_1)^2(2b_2)^2(5a_1)^2 \quad (1)$$

where [core] stands for

$$[\text{core}] = (1a_1)^2(2a_1)^2(1b_1)^2(1b_2)^2(3a_1)^2 \quad (2)$$

However, this electronic state may be more appropriately represented by the two-configuration wave function

$$C_1[\text{core}](4a_1)^2(2b_2)^2(5a_1)^2 + C_2[\text{core}](4a_1)^2(2b_2)^2(2b_1)^2 \quad (3)$$

where the CI coefficients are of opposite sign with $|C_1| > |C_2|$. Unlike the ground state, the first two excited states are adequately described by a single dominant configuration. The first excited state of AlH_2^- is an open-shell triplet which may be written as

$$[\text{core}](4a_1)^2(2b_2)^2(5a_1)(2b_1) {}^3B_1 \quad (4)$$

The second excited state, the last examined in the research, is the open-shell singlet in which the spins of the two unpaired electrons in the 3B_1 state become oriented opposite one another

$$[\text{core}](4a_1)^2(2b_2)^2(5a_1)(2b_1) {}^1B_1 \quad (5)$$

III. Theoretical Procedures

A. Basis Sets. Five basis sets of triple- ζ quality in the valence space were employed in the investigation of AlH_2^- . With the exception of the largest set, they were all modifications of a TZ2P basis set consisting of the McLean–Chandler triple- ζ (12s9p/6s5p) contraction of Huzinaga's primitive Gaussian set for aluminum^{19,20} augmented by two sets of d-type polarization functions with orbital exponents $\alpha_d(\text{Al}) = 0.80$ and 0.20 and the Huzinaga–Dunning triple- ζ (5s/3s) contracted set for hydrogen^{21,22} augmented by two sets of p-type polarization functions with orbital exponents $\alpha_p(\text{H}) = 1.50$ and 0.375 . The smallest basis set employed, designated TZ2P+diff, contained 55 basis functions and consisted of the TZ2P basis augmented with a set of s-type and p-type diffuse functions added to aluminum ($\alpha_s(\text{Al}) = 0.01703$ and $\alpha_p(\text{Al}) = 0.01497$) and an s-type diffuse function added to hydrogen ($\alpha_s(\text{H}) = 0.03016$). The TZ2P+diff basis set was further augmented by adding on a second set of s-type and p-type diffuse functions to aluminum ($\alpha_s(\text{Al}) = 0.005366$ and $\alpha_p(\text{Al}) = 0.005418$) and another s-type diffuse function to hydrogen ($\alpha_s(\text{H}) = 0.009247$). The next two basis sets in size were formed by augmenting the TZ2P+diff and TZ2P+2diff sets through the addition of a set of f-type polarization functions to aluminum ($\alpha_f(\text{Al}) = 0.25$) and a set of d-type polarization functions to hydrogen ($\alpha_d(\text{H}) = 1.0$), giving basis sets denoted TZ2P(f,d)+diff and TZ2P(f,d)+2diff, respectively. The largest basis set, TZ3P(2f,2d)+2diff, differed from its smaller brethren and used triple polarization instead of double ($\alpha_d(\text{Al}) = 1.60, 0.40$, and 0.10 ; $\alpha_p(\text{H}) = 3.0, 0.75$, and 0.1875). At 106 functions, the TZ3P(2f,2d)+2diff basis also included two sets of higher angular momentum functions on hydrogen and aluminum ($\alpha_f(\text{Al}) = 0.50$ and 0.125 ; and $\alpha_d(\text{H}) = 2.0$ and 0.5) as well as the two aforementioned sets of diffuse functions. Pure angular momentum (5d, 7f) functions were used throughout.

B. Methods. The zeroth-order description of the three lowest electronic states may be obtained using single-configuration self-consistent-field (SCF) wave functions. However, a more appropriate description of the $\tilde{X} {}^1A_1$ state was obtained by the first eigenvector (eq 3) of the TCSCF secular equation. At the TCSCF equilibrium geometry with the TZ3P(2f,2d)+2diff basis set, the configuration interaction coefficients were $C_1 = 0.969$

and $C_2 = -0.246$. Geometries of the first two excited states were optimized via standard analytic derivative methods at the SCF²³ and configuration interaction including single and double excitations (CISD)^{24–27} levels of theory. The geometry of the ground state was optimized using analytic derivatives of the TCSCF²³ and TCSCF-CISD²⁸ wave functions. In all cases, residual internal coordinate gradients were less than 10^{-6} in atomic units. Harmonic vibrational frequencies and associated infrared (IR) intensities were determined analytically at both the SCF^{29–32} and TCSCF³³ levels of theory and by finite differences of analytic gradients for the CISD wave functions. All calculations were performed using the PSI³⁴ suite of quantum chemistry programs.

Dynamical correlation effects were determined beyond the CISD level by application of CASSCF and CASSCF second-order configuration interaction (SOC) levels of theory at the CISD-optimized geometries. In all CISD and SOC procedures, the core (Al 1s-, 2s-, and 2p-like) orbitals were constrained to be doubly occupied and a single virtual (Al 1s*-like) orbital was deleted. With the TZ3P(2f,2d)+2diff basis set, the number of configuration state functions (CSFs) included in the CISD wave functions in C_{2v} symmetry are 21 593 ($\tilde{X} {}^1A_1$, TCSCF reference), 16 036 ($\tilde{a} {}^3B_1$, SCF reference), and 15 971 ($\tilde{A} {}^1B_1$, SCF reference). Two CASSCF wave functions with different active spaces were constructed for each state. The first, denoted CAS I, had an active space comprised of six valence electrons distributed among six valence orbitals (6 $e^-/6$ MO). The number of CSFs in the CAS I wave functions for the three states in C_{2v} symmetry were 56 ($\tilde{X} {}^1A_1$), 51 ($\tilde{a} {}^3B_1$), and 39 ($\tilde{A} {}^1B_1$), respectively. This choice of active space is equivalent to that used by Cramer and co-workers,¹⁸ although they report the number of CSFs in C_1 symmetry. The second CASSCF wave function, denoted CAS II, possessed an active space comprised of the CAS I active space augmented by inclusion of the $7a_1$, $3b_2$, and $4b_2$ virtual orbitals, resulting in an active space of 6 electrons distributed among 9 molecular orbitals (6 $e^-/9$ MO). The importance of the three additional virtual orbitals was observed in the more rapid convergence of the CAS II wave function and by the energy of the three orbitals as expressed in the SCF and TCSCF wave functions when diffuse functions were added to the basis set. With the larger active space, the number of CSFs in the CAS II wave functions for the three states in C_{2v} symmetry were 684 ($\tilde{X} {}^1A_1$), 864 ($\tilde{a} {}^3B_1$), and 608 ($\tilde{A} {}^1B_1$), respectively.

In conjunction with the choice of two active spaces for the CASSCF wave functions, two CASSCF-based SOC wave functions were constructed for each state. The first, denoted CAS I SOC, included all single and double excitations out of the CAS I references. With the TZ3P(2f,2d)+2diff basis set, the number of CSFs in the CAS I SOC wave functions in C_{2v} symmetry for the three states were 241 570 ($\tilde{X} {}^1A_1$), 366 305 ($\tilde{a} {}^3B_1$), and 232 801 ($\tilde{A} {}^1B_1$), respectively. The second, denoted CAS II SOC, included all single and double excitations out of the CAS II reference. With the same basis set, the number of CSFs in the CAS II SOC wave functions in C_{2v} symmetry for the three states were 1 265 238 ($\tilde{X} {}^1A_1$), 2 043 652 ($\tilde{a} {}^3B_1$), and 1 243 520 ($\tilde{A} {}^1B_1$), respectively.

IV. Results and Discussion

The ground and first two excited states of AlH_2^- were predicted to have bent equilibrium geometries with equivalent Al–H bond lengths, i.e. all structures possess C_{2v} symmetry. Tables 1–3 contain both (TC)SCF and (TC)CISD predictions of the total energy, equilibrium geometry, dipole moment,

TABLE 1: Two-Reference Configuration Theoretical Predictions of the Total Energy (in Hartrees, Subtract 240), Bond Lengths (in Å), Bond Angles (in degrees), Dipole Moments (in Debyes), Harmonic Vibrational Frequencies (in cm^{-1}), Infrared Intensities (in parentheses, km/mol), and Zero-Point Vibrational Energies (ZPVE in kcal/mol) for the \tilde{X}^1A_1 State of the AlH_2^- Molecule

level of theory	energy	r_e	θ_e	μ_e	$\omega_1(a_1)$	$\omega_2(a_1)$	$\omega_3(b_2)$	ZPVE
TZ2P+diff TCSCF	-3.047397	1.6865	96.80	0.5309	1534 (1656.2)	861 (561.0)	1506 (1197.6)	5.577
TZ2P+2diff TCSCF	-3.047609	1.6866	96.92	0.3904	1534 (1620.3)	861 (562.4)	1506 (1176.9)	5.578
TZ2P(f,d)+diff TCSCF	-3.048714	1.6856	96.99	0.5635	1540 (1616.8)	864 (573.2)	1511 (1190.0)	5.596
TZ2P(f,d)+2diff TCSCF	-3.048914	1.6857	97.10	0.4314	1540 (1591.1)	865 (569.0)	1511 (1168.7)	5.597
TZ3P(2f,2d)+2diff TCSCF	-3.051237	1.6806	97.49	0.6971	1554 (1510.3)	859 (498.4)	1528 (1137.2)	5.633
TZ2P+diff TC-CISD	-3.141610	1.6871	95.25	0.5218	1511 (1579.2)	826 (538.1)	1496 (1014.5)	5.478
TZ2P+2diff TC-CISD	-3.141801	1.6873	95.32	0.3750	1510 (1566.3)	825 (539.6)	1496 (997.3)	5.477
TZ2P(f,d)+diff TC-CISD	-3.148835	1.6837	95.37	0.6165	1514 (986.9)	829 (523.0)	1529 (1484.4)	5.536
TZ2P(f,d)+2diff TC-CISD	-3.149013	1.6840	95.45	0.4770	1514 (967.8)	829 (520.1)	1528 (1477.3)	5.534
TZ3P(2f,2d)+2diff TC-CISD	-3.153698	1.6809	95.60	0.6414	1533 (1407.5)	819 (441.8)	1520 (968.8)	5.536
Mod-aug-cc-pVTZ CAS(6,6) ^a		1.719	96.6		1401	784	1384	

^a Cramer, C. J.; Dulles, F. J.; Storer, J. W.; Worthington, S. E. *Chem. Phys. Lett.* **1994**, *218*, 387.

TABLE 2: Single-Reference Configuration Theoretical Predictions of the Total Energy (in Hartrees, Subtract 240), Bond Lengths (in Å), Bond Angles (in degrees), Dipole Moments (in Debye), Harmonic Vibrational Frequencies (in cm^{-1}), Infrared Intensities (in parentheses, km/mol), and Zero-Point Vibrational Energies (ZPVE in kcal/mol) for the \tilde{a}^3B_1 State of the AlH_2^- Molecule

level of theory	energy	r_e	θ_e	μ_e	$\omega_1(a_1)$	$\omega_2(a_1)$	$\omega_1(b_2)$	ZPVE
TZ2P+diff SCF	-3.031523	1.6122	117.96	0.3636	1811 (325.9)	783 (386.3)	1814 (666.5)	6.302
TZ2P+2diff SCF	-3.031881	1.6112	118.05	0.3598	1812 (310.4)	785 (391.2)	1821 (641.5)	6.316
TZ2P(f,d)+diff SCF	-3.032209	1.6121	117.98	0.3606	1812 (328.7)	784 (385.7)	1816 (669.1)	6.307
TZ2P(f,d)+2diff SCF	-3.032545	1.6111	118.06	0.3575	1813 (313.4)	786 (390.4)	1822 (644.9)	6.320
TZ3P(2f,2d)+2diff SCF	-3.034090	1.6112	117.18	0.1039	1812 (314.5)	782 (296.0)	1816 (619.0)	6.306
TZ2P+diff CISD	-3.121160	1.6175	118.14	0.3180	1757 (279.7)	744 (339.6)	1770 (576.3)	6.314
TZ2P+2diff CISD	-3.121445	1.6173	118.18	0.3237	1760 (276.9)	745 (345.5)	1772 (560.9)	6.114
TZ2P(f,d)+diff CISD	-3.127740	1.6164	118.22	0.2840	1768 (273.5)	742 (332.7)	1781 (562.2)	6.134
TZ2P(f,d)+2diff CISD	-3.127978	1.6163	118.25	0.2904	1770 (272.6)	742 (339.0)	1782 (548.5)	6.139
TZ3P(2f,2d)+2diff CISD	-3.132446	1.6165	117.79	0.0281	1769 (288.8)	737 (261.7)	1777 (535.1)	6.122
Mod-aug-cc-pVTZ CAS(6,6) ^a		1.644	117.2		1656	706	1646	

^a Cramer, C. J.; Dulles, F. J.; Storer, J. W.; Worthington, S. E. *Chem. Phys. Lett.* **1994**, *218*, 387.

TABLE 3: Single-Reference Configuration Theoretical Predictions of the Total Energy (in Hartrees, Subtract 240), Bond Lengths (in Å), Bond Angles (in degrees), Dipole Moments (in Debye), Harmonic Vibrational Frequencies (in cm^{-1}), Infrared Intensities (in parentheses, km/mol), and Zero-Point Vibrational Energies (ZPVE in kcal/mol) for the \tilde{A}^1B_1 State of the AlH_2^- Molecule

level of theory	energy	r_e	θ_e	μ_e	$\omega_1(a_1)$	$\omega_2(a_1)$	$\omega_3(b_2)$	ZPVE
TZ2P+diff SCF	-3.006788	1.5940	119.04	0.5333	1909 (132.1)	807 (232.0)	1918 (440.7)	6.625
TZ2P+2diff SCF	-3.020441	1.5880	118.62	0.4020	1942 (113.1)	821 (239.5)	1952 (364.8)	6.741
TZ2P(f,d)+diff SCF	-3.007507	1.5939	119.10	0.5224	1912 (131.8)	807 (233.0)	1920 (438.4)	6.631
TZ2P(f,d)+2diff SCF	-3.021006	1.5878	118.63	0.4022	1945 (113.6)	821 (239.9)	1954 (363.4)	6.748
TZ3P(2f,2d)+2diff SCF	-3.021954	1.5866	118.53	0.2154	1948 (122.5)	821 (231.1)	1957 (360.1)	6.756
TZ2P+diff CISD	-3.093051	1.6065	119.59	0.5037	1797 (110.7)	750 (195.7)	1831 (410.8)	6.260
TZ2P+2diff CISD	-3.101494	1.5959	118.63	0.3591	1857 (87.5)	778 (198.8)	1887 (304.5)	6.464
TZ2P(f,d)+diff CISD	-3.099635	1.6059	119.76	0.4607	1806 (105.9)	748 (193.9)	1841 (401.4)	6.284
TZ2P(f,d)+2diff CISD	-3.107358	1.5951	118.66	0.3351	1867 (84.3)	778 (194.8)	1898 (295.3)	6.494
TZ3P(2f,2d)+2diff CISD	-3.109852	1.5944	118.65	0.2383	1867 (97.5)	772 (180.8)	1897 (302.2)	6.484

harmonic vibrational frequencies and associated infrared (IR) intensities, and zero-point vibrational energy (ZPVE) of the \tilde{X}^1A_1 , \tilde{a}^3B_1 , and \tilde{A}^1B_1 electronic states, respectively. In all cases, the dipole moment was determined with respect to the center of mass. Table 4 contains CASSCF and SOCI predictions, using both the CAS I and CAS II active spaces, of total energies for all three electronic states at their CISD equilibrium geometries. The last two Tables 5 and 6, provide relative energies of the first two excited states with respect to the ground state (T_e values). Tables 5 and 6 also present ZPVE-corrected energy separations (T_0 values). At the CASSCF and SOCI levels of theory, where a vibrational frequency determination was not performed, the ZPVE correction was estimated by using the CISD harmonic vibrational frequencies with the same basis set.

A. Geometries. Regarding theoretical geometries and predictions of physical properties, especially when no experimental data are available, it is important to be aware of trends associated

with both basis set size and the level of electron correlation. Therefore, when feasible, one should employ several basis sets which contain different numbers of diffuse, higher angular momentum, and polarization functions. In general, expanding the basis set contracts bond lengths whereas employing more complete treatments of electron correlation tends to have the opposite effect and, thus, may lead to a fortuitous cancellation of errors. Hence, a smaller basis set at a given level of electron correlation may predict an equilibrium geometry closer to experiment than a larger basis set but may not do as well for energetics. Therefore, while the use of the TZ3P(2f,2d)+2diff basis set in conjunction with the CISD method for AlH_2^- may underestimate bond lengths and bond angles, it is important to examine trends in progressing to a basis set this large. This is especially important in CASSCF-SOCI procedures to determine if theoretically predicted energy separations between states are convergent and stable.

TABLE 4: Total CASSCF (CAS I and CAS II) and CASSCF SOCI Energies (in Hartrees, Subtract 240) at the CISD-Optimized Geometries for the Three Lowest Electronic States of AlH_2^-

level of theory	\tilde{X}^1A_1	\tilde{a}^3B_1	\tilde{A}^1B_1
TZ2P+diff CAS I	-3.074534	-3.059544	-3.035554
TZ2P+2diff CAS I	-3.074737	-3.059890	-3.048712
TZ2P(f,d)+diff CAS I	-3.075725	-3.060158	-3.036246
TZ2P(f,d)+2diff CAS I	-3.075917	-3.060486	-3.049233
TZ3P(2f,2d)+2diff CAS I	-3.078128	-3.061876	-3.050149
TZ2P+diff CAS I SOCI	-3.144863	-3.124487	-3.096911
TZ2P+2diff CAS I SOCI	-3.145051	-3.124763	-3.104177
TZ2P(f,d)+diff CAS I SOCI	-3.152272	-3.131282	-3.103758
TZ2P(f,d)+2diff CAS I SOCI	-3.152446	-3.131505	-3.110155
TZ3P(2f,2d)+2diff CAS I SOCI	-3.157361	-3.136256	-3.112852
TZ2P+diff CAS II	-3.090670	-3.077567	-3.052619
TZ2P+2diff CAS II	-3.092338	-3.077957	-3.065426
TZ2P(f,d)+diff CAS II	-3.093605	-3.078841	-3.054137
TZ2P(f,d)+2diff CAS II	-3.093765	-3.079211	-3.066974
TZ3P(2f,2d)+2diff CAS II	-3.095799	-3.080790	-3.067809
TZ2P+diff CAS II SOCI	-3.146717	-3.125953	-3.099362
TZ2P+2diff CAS II SOCI	-3.146932	-3.126240	-3.105453
TZ2P(f,d)+diff CAS II SOCI	-3.154371	-3.132931	-3.106673
TZ2P(f,d)+2diff CAS II SOCI	-3.154545	-3.133175	-3.111751
TZ3P(2f,2d)+2diff CAS II SOCI	-3.159682	-3.138201	-3.115001

TABLE 5: Relative Energies T_c (in kcal/mol, T_0 in parentheses) of the Three Lowest-Lying Electronic States of AlH_2^- at the SCF, TCSCF, CASSCF (CAS I and CAS II) Levels of Theory

level of theory	\tilde{X}^1A_1	\tilde{a}^3B_1	\tilde{A}^1B_1
TZ2P+diff (TC)SCF	0.0	9.961 (10.686)	25.483 (26.531)
TZ2P+2diff (TC)SCF	0.0	9.869 (10.607)	17.048 (18.211)
TZ2P(f,d)+diff (TC)SCF	0.0	10.357 (11.068)	25.858 (26.893)
TZ2P(f,d)+2diff (TC)SCF	0.0	10.272 (10.995)	17.513 (18.664)
TZ3P(2f,2d)+2diff (TC) SCF	0.0	10.760 (11.433)	18.375 (19.498)
TZ2P+diff CAS I	0.0	9.406 (10.242)	24.460 (25.242)
TZ2P+2diff CAS I	0.0	9.317 (9.954)	16.331 (17.318)
TZ2P(f,d)+diff CAS I	0.0	9.768 (10.366)	24.773 (25.521)
TZ2P(f,d)+2diff CAS I	0.0	9.683 (10.288)	16.744 (17.704)
TZ3P(2f,2d)+2diff CAS I	0.0	10.198 (10.784)	17.557 (18.505)
TZ2P+diff CAS II	0.0	8.222 (9.058)	23.877 (24.659)
TZ2P+2diff CAS II	0.0	9.024 (9.661)	16.888 (17.875)
TZ2P(f,d)+diff CAS II	0.0	9.265 (9.863)	24.767 (25.515)
TZ2P(f,d)+2diff CAS II	0.0	9.133 (9.738)	16.812 (17.772)
TZ3P(2f,2d)+2diff CAS II	0.0	9.418 (10.004)	17.564 (18.512)

TABLE 6: Relative Energies T_c (in kcal/mol, T_0 in parentheses) of the Three Lowest-Lying Electronic States of AlH_2^- at the CISD and SOCI (CAS I and CAS II references) Levels of Theory

level of theory	X^1A_1	\tilde{a}^3B_1	\tilde{A}^1B_1
TZ2P+diff (TC)CISD	0.0	12.833 (13.669)	30.471 (31.253)
TZ2P+2diff (TC)CISD	0.0	12.774 (13.411)	25.293 (26.280)
TZ2P(f,d)+diff (TC)CISD	0.0	13.237 (13.835)	30.873 (31.621)
TZ2P(f,d)+2diff (TC)CISD	0.0	13.200 (13.805)	26.139 (27.099)
TZ3P(2f,2d)+2diff (TC)CISD	0.0	13.336 (13.922)	27.514 (28.462)
TZ2P+diff CAS I SOCI	0.0	12.786 (13.622)	30.090 (30.872)
TZ2P+2diff CAS I SOCI	0.0	12.731 (13.368)	25.649 (26.636)
TZ2P(f,d)+diff CAS I SOCI	0.0	13.171 (13.769)	30.443 (31.191)
TZ2P(f,d)+2diff CAS I SOCI	0.0	13.141 (13.746)	26.538 (27.498)
TZ3P(2f,2d)+2diff CAS I SOCI	0.0	13.244 (13.830)	27.930 (28.878)
TZ2P+diff CAS II SOCI	0.0	13.030 (13.866)	29.716 (30.498)
TZ2P+2diff CAS II SOCI	0.0	12.984 (13.621)	26.028 (27.015)
TZ2P(f,d)+diff CAS II SOCI	0.0	13.454 (14.052)	29.931 (30.679)
TZ2P(f,d)+2diff CAS II SOCI	0.0	13.410 (14.015)	26.854 (27.814)
TZ3P(2f,2d)+2diff CAS II SOCI	0.0	13.480 (14.066)	28.038 (28.986)
Mod-aug-cc-pVTZ MRCISD(Q) ^a	0.0	13.7 (14.3)	

^a Cramer, C. J.; Dulles, F. J.; Storer, J. W.; Worthington, S. E. *Chem. Phys. Lett.* **1994**, 218, 387.

Examining trends in bond lengths and bond angles upon progressing from the SCF to CISD levels of theory for a particular basis set, one observes that the predicted bond lengths of the \tilde{X}^1A_1 , \tilde{a}^3B_1 , and \tilde{A}^1B_1 states of AlH_2^- follow the anticipated trend and elongate. However, the change in bond length was small, typically no more than 0.02 Å. The bond

angles of the \tilde{a}^3B_1 and \tilde{A}^1B_1 states were consistently observed to widen upon progressing from SCF to CISD, typically by less than 0.2° but by at most 0.6°. Predictions of the ground state bond angle exhibited the opposite trend and were more sensitive to the correlation treatment, the bond angle closing by as much as 1.9° upon going from SCF to CISD. Comparing to the

CASSCF-optimized geometries of Cramer et al.,¹⁸ one observes that the CASSCF predictions for the Al–H bond lengths of the ground and \tilde{a}^3B_1 states are significantly longer than any of the CISD predictions, in accord with the expectation that the CASSCF method overestimates bond lengths due to the exaggerated importance of the antibonding orbitals in the active space. For the ground state, the CASSCF method predicted a bond angle wider than any of the (TC)CISD predictions, whereas for the \tilde{a}^3B_1 excited state, the CASSCF method predicts a somewhat smaller bond angle.

In addition to examining the impact of the correlation treatment on the predicted equilibrium geometries, one should also investigate the effects of expanding the basis set. At the (TC)SCF and (TC)CISD levels of theory, the addition of a second set of diffuse functions to the TZ2P+diff or TZ2P-(f,d)+diff basis sets had little effect on the bond angles and bond lengths of the \tilde{X}^1A_1 and \tilde{a}^3B_1 states predicted by these basis sets, causing at most a 0.001 Å change in bond length and a 0.12° change in bond angle. The equilibrium geometry of the A^1B_1 state was more sensitive to the addition of the second set of diffuse functions at the CISD level, exhibiting a 0.01 Å decrease in bond length and a 1.1° decrease in bond angle. The addition of higher angular momentum functions to either the TZ2P+diff and TZ2P+2diff basis sets had little visible effect on bond lengths and angles predicted at the (TC)SCF and (TC)CISD levels, the maximum change being 0.0034 Å in the bond length and 0.13° in the bond angle. Lastly, adding a set of higher angular momentum functions to the TZ2P-(f,d)+2diff basis set and swapping double for triple polarization, producing the largest basis set [TZ3P(2f,2d)+2diff], altered the TZ2P(f,d)+2diff predictions of bond lengths by at most 0.005 Å and bond angles by a comparatively large 0.9°.

Next, one can examine changes in the TZ3P(2f,2d)+2diff (TC)CISD predictions of bond lengths and angles upon excitation from the ground state to the first two excited states. Note that, in general, the observed trends also hold for the smaller basis sets but not necessarily with the same magnitudes. In order of increasing Al–H bond length, the three states are observed to follow the sequence



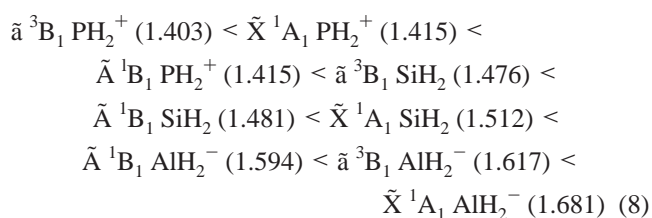
Whereas in order of increasing bond angle, the three states followed the opposite sequence



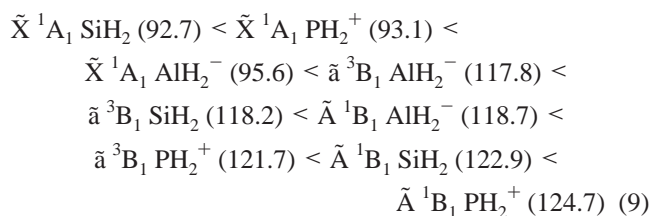
The trend in the bond angles may be, in part, explained with the aid of the Walsh diagram for an XH_2 molecule,³⁵ where X indicates any heavy atom. In the Walsh diagram, the “binding energies” of the valence orbitals are plotted against the bond angle, providing a rough qualitative picture of each orbital’s impact on the overall molecular geometry. In the case of AlH_2^- , the Walsh diagram indicates that the $4a_1$ and $2b_2$ orbitals both energetically prefer a linear structure whereas the $5a_1$ orbital strongly prefers a bent structure and the $2b_1$ orbital shows almost no preference. The $4a_1$ and $2b_2$ orbitals are filled in all three electronic states, and therefore, it is the influence of the $5a_1$ and $2b_1$ orbitals which serves to distinguish the geometry of the three states. In the ground state, the $5a_1$ orbital is doubly occupied and clearly dominates, which is in accord with the heavily bent bond angle of 95.6°. The first two excited states both differ from the ground state by the excitation of a single electron from the $5a_1$ orbital into the $2b_1$ orbital, which weakens the influence of the $5a_1$ orbital, causing the bond angle to open

as observed. The two excited states have the same orbital occupation and only differ in spin symmetry, and thus according to the Walsh diagram, they should have similar bond angles. At the TZ3P(2f,2d)+2diff CISD level, the bond angle of the two excited states is indeed close, differing by only 0.86°. The opposite trends in bond length and bond angle may now be rationalized in terms of the interaction of the hydrogen atoms. In the ground state, the small angle forces the two hydrogen atoms close together and in response the Al–H bonds elongate in order to reduce their repulsive interaction, whereas in the two excited states, each with wider bond angles, the H–H repulsive interactions are less and the Al–H bonds need not be as long.

Finally, it is informative to examine how the theoretical geometry of AlH_2^- compares relative to corresponding predictions on SiH_2^{15} and PH_2^+ ,¹⁶ two other second-row dihydrides isoelectronic to AlH_2^- and isovalent to methylene. The bond lengths of these three species are observed to follow the sequence (TZ3P(2f,2d)+2diff CISD values in Å, in parentheses)



From eq 8, it is apparent that a general trend exists in which P–H bond lengths are shorter than Si–H bond lengths, which are in turn shorter than the Al–H bond lengths. This trend in bond lengths may be explained by the charges and corresponding radii of the Al^- , Si, and P^+ species. With its extra electron, Al^- has the largest radius of the three species and the smallest electronegativity, neutral Si has an intermediate radius and electronegativity, and P^+ is electron deficient with the smallest radius. The bond angles of the three isoelectronic species were observed to exhibit the following trend (TZ3P(2f,2d)+2diff CISD values in degrees, in parenthesis):



B. Dipole Moments. At the (TC)SCF level of theory with the largest basis set employed, TZ3P(2f,2d)+2diff, the magnitudes (in debyes, D) of the dipole moments of the \tilde{X}^1A_1 , \tilde{a}^3B_1 , and \tilde{A}^1B_1 electronic states of AlH_2^- , determined relative to the center of mass, are 0.70, 0.10, and 0.22 D, respectively. With the same basis set, the effect of correlating all single and double excitations out of the (TC)SCF reference, (TC)CISD, was to decrease the dipole moments of the \tilde{X}^1A_1 and \tilde{a}^3B_1 states to 0.64 and 0.03 D, respectively, and to increase the dipole moment of the \tilde{A}^1B_1 state to 0.24 D. Note that this trend only occurred for the largest basis set. With most of the smaller basis sets, the dipole moment was observed to decrease with the inclusion of correlation; however, dipole moments can be sensitive to basis set, and there is no hard and fast rule. The dipole moments determined at the (TC)SCF and (TC)CISD levels of theory are all determined as energy derivatives with respect to electric field perturbation. For the ground state, the

dipole moment vector lies along the C_2 symmetry axis with the negative end located near the two hydrogen atoms. For the two excited states, \tilde{a}^3B_1 and \tilde{A}^1B_1 , the dipole moment changes sign with the negative end located near the aluminum atom.

The relatively large predicted dipole moment, 0.64 D, of the ground state of AlH_2^- indicates that if significant concentrations of the anion can be isolated in the gas phase, microwave spectroscopic investigations of this state might be possible. Conversely, the smaller dipole moments of the two excited states could hinder their investigation by microwave spectroscopy. The larger dipole moment of the ground state compared to the two excited states may be explained by the change in the position of the center of negative charge upon electronic excitation. In the ground state, the negative charge is spread almost equally among the three atoms, which places the center of negative charge closer to the two hydrogen atoms and farther away from the center of mass, giving a larger predicted dipole moment. In the two excited states, the majority of the negative charge resides on the aluminum atom which, due to its much greater mass, is essentially on top of the center of mass, yielding a smaller predicted dipole moment. Moreover, the equilibrium geometry of the ground state has a much smaller bond angle that serves to increase the components of the Al-H bond moments along the C_2 symmetry axis.

C. Harmonic Vibrational Frequencies. At the TZ3P(2f,-2d)+2diff CISD level of theory, the harmonic vibrational frequencies of the symmetric stretching mode (ω_1), bending mode (ω_2), and asymmetric stretching mode (ω_3) of AlH_2^- were predicted, in cm^{-1} , to be $\omega_1 = 1533$, $\omega_2 = 819$, and $\omega_3 = 1520$ for the ground state; $\omega_1 = 1769$, $\omega_2 = 737$, and $\omega_3 = 1777$ for the \tilde{a}^3B_1 state; and $\omega_1 = 1867$, $\omega_2 = 772$, and $\omega_3 = 1897$ for the \tilde{A}^1B_1 state. In accordance with Badger's well-known rule that stretching vibrational frequencies generally decrease with increasing bond length,^{36,37} the above harmonic stretching frequencies, either symmetric or asymmetric, were observed to follow the relative order

$$\tilde{X}^1A_1 < \tilde{a}^3B_1 < \tilde{A}^1B_1 \quad (10)$$

which is indeed opposite the observed trend in bond lengths shown in eq 6. At the TZ3P(2f,2d)+2diff CISD level of theory, the two harmonic stretching frequencies of the same three electronic states of SiH_2^{15} were also observed to follow Badger's rule and, therefore, differed from AlH_2^- in the relative order of the \tilde{a}^3B_1 and \tilde{A}^1B_1 frequencies. The situation was slightly different in the case of PH_2^+ at the same level of theory.¹⁶ The asymmetric stretching frequencies of the three lowest states of PH_2^+ were in accord with Badger's rule and ordered as follows

$$\tilde{A}^1B_1 < \tilde{X}^1A_1 < \tilde{a}^3B_1 \quad (11)$$

whereas the symmetric stretching frequency of the \tilde{X}^1A_1 state of PH_2^+ was predicted to be greater than that of the \tilde{a}^3B_1 state, violating Badger's rule. The violation is minor considering that the two states differ in bond length by only 0.01 Å. With respect to the harmonic bending frequency, the three lowest states of AlH_2^- are ordered as follows:

$$\tilde{a}^3B_1 < \tilde{A}^1B_1 < \tilde{X}^1A_1 \quad (12)$$

The greater bending frequency of the ground state relative to the two excited states is in accord with the usual expectation that smaller bond angles give rise to higher harmonic vibrational frequencies. The fact that the relative ordering of the bending

frequencies of the \tilde{a}^3B_1 and \tilde{A}^1B_1 states does not meet this expectation is not terribly surprising given the close similarity in their bond angles, which differ by less than 1°. In addition, the relative ordering of the three electronic states of AlH_2^- with respect to the bending frequency differs from that observed for SiH_2 and PH_2^+ , both of which followed the expected trend relating bond angle and bending frequency, in the relative ordering of the \tilde{a}^3B_1 and \tilde{A}^1B_1 states.

The magnitudes of symmetric stretching, asymmetric stretching, and bending harmonic vibrational frequencies of the second-row dihydrides isovalent to methylene follow a clear trend as the central atom progresses toward the right side of the periodic table: the value of all three increases. Consider, for example, the \tilde{X}^1A_1 ground states of AlH_2^- , SiH_2 , and PH_2^+ . At the TZ3P(2f,2d)+diff (TC)CISD level of theory, the symmetric stretching frequency increases by 570 cm^{-1} upon moving from AlH_2^- to SiH_2 and by a further 354 cm^{-1} from SiH_2 to PH_2^+ . The trend in the asymmetric stretching frequency was similar at this level of theory, increasing by 580 cm^{-1} from AlH_2^- to SiH_2 and by another 367 cm^{-1} upon moving to PH_2^+ . Lastly, the bending frequency went up by 217 cm^{-1} from AlH_2^- to SiH_2 and up by another 119 cm^{-1} upon going to PH_2^+ . The trends in harmonic vibrational frequencies for the first two excited states are similar, although typically a bit smaller. The observed trend in the two stretching frequencies is opposite that expected based on the masses alone and must, therefore, be due to the strength of the bond as expressed by the force constant. The decreasing bond length and increasing strength of the X-H bond (X = Al, Si, P) in the dihydrides may be explained by the charge state, electronegativity, and resultant radius of the central species (Al^- , Si, P^+).

Due to the lack of experimental data, it is difficult to ascertain the accuracy of the theoretically predicted harmonic vibrational frequencies presented here. However, one may gain some clues by examining the accuracy of these methods on similar systems by examining the convergence of the predictions with increasing basis set and by comparing them to the independently determined harmonic vibrational frequencies computed at the CASSCF level by Cramer et al.¹⁸ First, Yamaguchi et al.^{11,15} employed techniques identical to those used in this research to SiH_2 and CH_2 , two systems for which several of the fundamentals are experimentally known, and were able to determine that at the TZ3P(2f,2d)+2diff CISD level of theory there is an error of approximately 5% or less between the theoretical harmonic vibrational frequency and the experimental fundamental. In most cases, the theoretical prediction, which does not include anharmonic effects, will overestimate the fundamental. Second, CISD predictions of the harmonic vibrational frequencies of the ground and \tilde{a}^3B_1 states were found to be fairly insensitive to the choice of basis set, changing by at most 33 cm^{-1} for the ground state and 13 cm^{-1} for the \tilde{a}^3B_1 state. The \tilde{A}^1B_1 state was more sensitive to the basis set size, the stretching modes changing by as much as 70 cm^{-1} . However improving the TZ2P(f,d)+2diff basis set to give the TZ3P(2f,2d)+2diff set changed the harmonic vibrational frequency predictions of the \tilde{A}^1B_1 state by at most 6 cm^{-1} . Taken together, these facts suggest that for the three states the predicted harmonic vibrational frequencies are approaching their basis set limit values. Last, the CASSCF predictions of Cramer et al.¹⁸ for the ground and \tilde{a}^3B_1 states are qualitatively similar to our CISD predictions, giving the same relative order and magnitude, but are significantly smaller in overall magnitude. The lower CASSCF predictions of the stretching frequencies is to be expected, however, due to the CASSCF method's propensity

to overestimate bond lengths, as seen in the previous section, and thereby underestimate stretching frequencies.

D. Infrared (IR) Intensities. The symmetric stretching, bending, and asymmetric stretching vibrational modes of the three lowest electronic states of AlH_2^- all have associated IR intensities large enough to suggest that it should be possible to obtain IR spectra of the three states provided they can be produced in sufficient quantity. This last provision is not easy to fulfill, especially for the $\tilde{a}^3\text{B}_1$ and $\tilde{A}^1\text{B}_1$ states due to the electronically forbidden $\tilde{a}^3\text{B}_1 \leftarrow \tilde{X}^1\text{A}_1$ transition in the case of the former and the slightly lower adiabatic detachment threshold for the extra electron in the case of the latter. At the TZ3P(2f,-2d)+2diff CISD level of theory, the smallest IR intensity, 98 km mol^{-1} , occurred for the symmetric stretching frequency of the $\tilde{A}^1\text{B}_1$ state. Examining trends in the IR intensities of the three states, one observes that the IR intensity of each mode decreases on exciting from the ground state to the $\tilde{a}^3\text{B}_1$ state and yet again upon exciting from the $\tilde{a}^3\text{B}_1$ state to the $\tilde{A}^1\text{B}_1$ state. In order of increasing IR intensity at the TZ3P(2f,-2d)+2diff CISD level, the harmonic vibrational modes of the ground state follow the sequence ($\omega_2 < \omega_3 < \omega_1$) whereas the harmonic vibrational modes of the $\tilde{a}^3\text{B}_1$ state are in the order ($\omega_2 < \omega_1 < \omega_3$) and those of the $\tilde{A}^1\text{B}_1$ state in the order ($\omega_2 < \omega_3$).

E. Energetics. The relative energetic ordering of the three lowest electronic states of AlH_2^- was determined, at all levels of theory employed, to follow the same trend observed for the other second-row dihydrides, SiH_2^{15} and PH_2^+ ,¹⁶ namely



In the case of the isovalent first-row dihydrides, BH_2^- ,¹⁸ CH_2 ,³⁸ and NH_2^+ ,³⁹ the energetic ordering of the $^3\text{B}_1$ and 1^1A_1 electronic states is found to be switched relative to the order given in eq 13. The difference in the behavior of the first- and second-row dihydrides can be related to the degree of hybridization undergone by orbitals in the central atom. For first-row XH_2 compounds, the 2s and 2p orbitals of the central atom, X, are able to mix and produce hybrid orbitals oriented at angles greater than 90°. The Walsh diagram for an XH_2 molecule indicates that as the bond angle widens, the “binding” energy separation of the $3a_1$ and $1b_1$ orbitals decreases to the point where the $^3\text{B}_1$ state could drop below the 1^1A_1 state, as observed. For the second-row dihydrides, the ability of orbitals on the central atom to hybridize is much less, as evidenced by ground state bond angles all close to 90°. From the Walsh diagram, the “binding energy” of the $5a_1$ orbital in a strongly bent XH_2 molecule falls well below that of the $2b_1$ orbital and the 1^1A_1 state is clearly the ground state.

1. $\tilde{X}^1\text{A}_1-\tilde{a}^3\text{B}_1$ Separation. The TZ3P(2f,2d)+2diff CAS II SOCI prediction of the energy separation (T_e) between the $\tilde{X}^1\text{A}_1$ and $\tilde{a}^3\text{B}_1$ electronic states is 13.48 kcal mol^{-1} . Including the ZPVE correction based on the (TC)CISD frequencies increases the separation to $T_0 = 14.07 \text{ kcal mol}^{-1}$. In all cases, the ZPVE correction increased the magnitude of the energy separation by a small amount, typically by less than 1 kcal mol^{-1} . Using the same basis set and the smaller set of CAS I references in the SOCI procedure decreased the energy separation, both T_e and T_0 , by only 0.24 kcal mol^{-1} . Examining the trend in the CAS II SOCI T_e predictions with basis set shows that upon including higher angular momentum functions into the basis set, the energy separation was confined between the values of 13.41 and 13.48 kcal mol^{-1} . The small variation in the CAS II SOCI prediction of T_e lends confidence that the real value is close to the highest level prediction of 13.48 kcal mol^{-1} .

In their systematic study, Cramer et al.¹⁸ predicted a slightly larger T_e value of 13.7 kcal mol^{-1} ($T_0 = 14.3 \text{ kcal mol}^{-1}$). Predictions of the energy separation between the $\tilde{X}^1\text{A}_1$ and $\tilde{a}^3\text{B}_1$ states of SiH_2 and PH_2^+ with similar methods and basis sets were found to have achieved chemical accuracy, i.e., within 1 kcal mol^{-1} . Lastly, compared to the other second-row dihydrides (20.23 kcal mol^{-1} for SiH_2 and 17.89 kcal mol^{-1} for PH_2^+), AlH_2^- possesses the smallest separation between these two states.

2. $\tilde{X}^1\text{A}_1-\tilde{A}^1\text{B}_1$ Separation. At the TZ3P(2f, 2d)+2diff CAS II SOCI level of theory, the energy separation (T_e) between the ground and $\tilde{A}^1\text{B}_1$ state is predicted to be 28.04 kcal mol^{-1} . Adding the ZPVE correction based on the (TC)CISD frequencies increased the energy separation by 0.95 kcal mol^{-1} , yielding a prediction for T_0 of 28.99 kcal mol^{-1} . As with the $\tilde{X}^1\text{A}_1-\tilde{a}^3\text{B}_1$ separation, the ZPVE correction increased the gap between these two states by less than 1 kcal mol^{-1} . Performing the SOCI with the same basis set and the smaller set of CAS I references resulted in a 0.11 kcal mol^{-1} drop in the energy separation. The effect of the basis set on T_e was more pronounced for the CAS II SOCI predictions of the $\tilde{X}^1\text{A}_1-\tilde{A}^1\text{B}_1$ separation than for the $\tilde{X}^1\text{A}_1-\tilde{a}^3\text{B}_1$ separation. Among the four basis sets of TZ2P quality, the inclusion of the second set of diffuse functions decreased the separation by more than 3 kcal mol^{-1} whereas the effect of the higher angular momentum functions was to increase the gap by less than 1 kcal mol^{-1} . The largest basis set, TZ3P(2f,2d)+2diff, predicted a T_e value in the middle of those given by the four smaller basis sets, lending some credence that one is close to the true value. Predictions of the energy separation between the $\tilde{X}^1\text{A}_1$ and $\tilde{A}^1\text{B}_1$ states of SiH_2 and PH_2^+ with similar methods and basis sets were also found to have achieved chemical accuracy with error bars around 0.7 kcal mol^{-1} . Lastly, compared to the other second-row dihydrides (45.03 kcal mol^{-1} for SiH_2 and 46.37 kcal mol^{-1} for PH_2^+), AlH_2^- possesses the smallest separation between these two states.

3. Adiabatic Electron Detachment Energy. The G2 value for the adiabatic electron detachment energy (AEDE) of AlH_2^- is 1.15 eV (26.52 kcal mol^{-1})¹⁷ and is probably reliable to within 0.1 eV (2.3 kcal mol^{-1}). In order to compare with this value, the AEDE of AlH_2^- was determined at the (TC)SCF and (TC)-CISD levels of theory with the TZ3P(2f,2d)+2diff basis set. The (TC)SCF method severely underestimated the AEDE, predicting a value of only 0.51 eV (11.8 kcal mol^{-1}). Including the ZPVE correction increased this value by 0.05 eV (1.24 kcal mol^{-1}). At 0.95 eV (21.8 kcal mol^{-1}), the (TC)CISD prediction of the AEDE is much closer to the G2 value. Adding the ZPVE correction improves the agreement, giving our best prediction of 0.99 eV (22.8 kcal mol^{-1}).

The reason for computing the AEDE was not to challenge the G2 value but to determine the AEDE with levels of theory directly comparable to the energies of the $\tilde{a}^3\text{B}_1$ and $\tilde{A}^1\text{B}_1$ excited states found in this research. The adiabatic electron detachment threshold of AlH_2^- has little consequence for the ground and $\tilde{a}^3\text{B}_1$ states, which are both well below it, but the $\tilde{A}^1\text{B}_1$ state is predicted to lie above this threshold at the TZ3P(2f,2d)+2diff SCF and CISD levels. Indeed, the TZ3P(2f,-2d)+2diff CISD prediction for the energy of the $\tilde{A}^1\text{B}_1$ state is even above the larger G2 prediction of the adiabatic electron detachment threshold. Moreover, the orbital energy of the $2b_1$ orbital of the $\tilde{A}^1\text{B}_1$ state is slightly positive at the SCF level, indicating that at this level of theory the electron is not bound. The consequence is that the $\tilde{A}^1\text{B}_1$ state may not be of chemical significance because energy sufficient to reach this state may

detach the extra electron giving neutral AlH_2 . However, this state could be observed as a resonance in a scattering experiment. This result was not unexpected, for it is rare to have anions with even one excited state, but the $\tilde{\text{A}}^1\text{B}_1$ state was examined to make sure of its energy at high levels of theory with ZPVE corrections.

V. Conclusions

Three low-lying electronic states ($\tilde{\text{X}}^1\text{A}_1$, $\tilde{\text{a}}^3\text{B}_1$, and $\tilde{\text{A}}^1\text{B}_1$) of AlH_2^- were systematically investigated using high levels of ab initio electronic structure theory with the goal of providing reliable energetic and spectroscopic parameters. These investigations were carried out with a series of increasingly larger basis sets in order to gauge the convergence of predicted properties and provide theoreticians with an abundance of information to aid in making reliable estimates about energetic and geometric properties when very high levels of theory and large basis sets cannot be used. All three electronic states of AlH_2^- were predicted to possess bent equilibrium geometries with C_{2v} symmetry. At the TZ3P(2f,2d)+2diff (TC)CISD level, the highest level of theory at which a geometry optimization was performed, the equilibrium geometries of the three states were predicted to be $r_e = 1.681 \text{ \AA}$ and $\theta_e = 95.6^\circ$ ($\tilde{\text{X}}^1\text{A}_1$), $r_e = 1.617 \text{ \AA}$ and $\theta_e = 117.8^\circ$ ($\tilde{\text{a}}^3\text{B}_1$), and $r_e = 1.594 \text{ \AA}$ and $\theta_e = 118.7^\circ$ ($\tilde{\text{A}}^1\text{B}_1$). The energy separations (T_0) between the ground ($\tilde{\text{X}}^1\text{A}_1$) and first two excited states predicted at the CAS II SOCI level with the TZ3P(f,d)+2diff basis set were 14.1 ($\tilde{\text{a}}^3\text{B}_1 \leftarrow \tilde{\text{X}}^1\text{A}_1$) and 29.0 kcal mol $^{-1}$ ($\tilde{\text{A}}^1\text{B}_1 \leftarrow \tilde{\text{X}}^1\text{A}_1$). On the basis of previous work on SiH_2 and PH_2^+ where these methods were employed, it is estimated that predictions of the energy separations between states should be of chemical accuracy, i.e., within 1 kcal mol $^{-1}$.

Acknowledgment. The authors thank Jon Rienstra-Kiracofe for helpful suggestions and advice. This research was supported by the U.S. National Science Foundation, Grant No. CHE-9815397.

References and Notes

- Herzberg, G. *Proc. R. Soc. London Ser. A* **1961**, 262, 291.
- Foster, J. M.; Boys, S. F. *Rev. Mod. Phys.* **1960**, 32, 305.
- Bender, C. F.; Schaefer, H. F. *J. Am. Chem. Soc.* **1970**, 92, 4984–4985.
- Petek, H.; Nesbitt, D. J.; Moore, C. B.; Birss, F. W.; Ramsay, D. A. *J. Chem. Phys.* **1987**, 86, 1189.
- Duxbury, G.; Jungen, C. *Mol. Phys.* **1988**, 63, 981.
- Jensen, P.; Bunker, P. R. *J. Chem. Phys.* **1988**, 89, 1327.
- Comeau, D. C.; Shavitt, I.; Jensen, P.; Bunker, P. R. *J. Chem. Phys.* **1989**, 90, 6491–6500.
- Petek, H.; Nesbitt, D. J.; Darwin, D. C.; Ogilby, P. R.; Moore, C. B.; Ramsay, D. A. *J. Chem. Phys.* **1989**, 91, 6566.
- Green, W. H.; Handy, N. C.; Knowles, P. J.; Carter, S. *J. Chem. Phys.* **1991**, 94, 118.
- Woon, D. E.; Dunning, T. H. *J. Chem. Phys.* **1995**, 103, 4572.
- Yamaguchi, Y.; Sherrill, C. D.; Schaefer, H. F. *J. Phys. Chem.* **1996**, 100 (19), 7911.
- Shavitt, I. *Tetrahedron* **1985**, 41, 1531.
- Davidson, E. R.; Feller, D.; Phillips, P. *Chem. Phys. Lett.* **1980**, 76, 416.
- Handy, N. C.; Yamaguchi, Y.; Schaefer, H. F. *J. Chem. Phys.* **1986**, 84, 4481–4484.
- Yamaguchi, Y.; Van Huis, T. J.; Sherrill, C. D.; Schaefer, H. F. *Theor. Chem. Acc.* **1997**, 97, 341.
- Van Huis, T. J.; Yamaguchi, Y.; Sherrill, C. D.; Schaefer, H. F. *J. Phys. Chem.* **1997**, 101 (37), 6955.
- Mayer, P. M.; Radom, L. *J. Phys. Chem.* **1998**, 102, 4918.
- Cramer, C. J.; Dulles, F. J.; Storer, J. W.; Worthington, S. E. *Chem. Phys. Lett.* **1994**, 218 (5–6), 387.
- McLean, A. D.; Chandler, G. S. *J. Chem. Phys.* **1980**, 72, 5639.
- Huzinaga, S. *Approximate Atomic Wavefunctions*; Department of Chemistry: University of Alberta, 1971; Vol. II.
- Huzinaga, S. *J. Chem. Phys.* **1965**, 42, 1293.
- Dunning, T. H. *J. Chem. Phys.* **1971**, 55, 716.
- Goddard, J. D.; Handy, N. C.; Schaefer, H. F. *J. Chem. Phys.* **1979**, 71, 1525.
- Brooks, B. R.; Laidig, W. D.; Saxe, P.; Goddard, J. D.; Yamaguchi, Y.; Schaefer, H. F. *J. Chem. Phys.* **1980**, 72, 4652.
- Osamura, Y.; Yamaguchi, Y.; Schaefer, H. F. *J. Chem. Phys.* **1981**, 75, 2919.
- Osamura, Y.; Yamaguchi, Y.; Schaefer, H. F. *J. Chem. Phys.* **1982**, 77, 383–390.
- Rice, J. E.; Amos, R. D.; Handy, N. C.; Lee, T. J.; Schaefer, H. F. *J. Chem. Phys.* **1986**, 85, 963–968.
- Lee, T. J.; Allen, W. D.; Schaefer, H. F. *J. Chem. Phys.* **1987**, 87, 7062–7075.
- Saxe, P.; Yamaguchi, Y.; Schaefer, H. F. *J. Chem. Phys.* **1982**, 77, 5647–5654.
- Osamura, Y.; Yamaguchi, Y.; Saxe, P.; Vincent, M. A.; Gaw, J. F.; Schaefer, H. F. *J. Chem. Phys.* **1982**, 72, 131.
- Osamura, Y.; Yamaguchi, Y.; Saxe, P.; Fox, D. J.; Vincent, M. A.; Schaefer, H. F. *J. Mol. Struct. (Theochem)* **1983**, 103, 183.
- Yamaguchi, Y.; Frisch, M. J.; Gaw, J. F.; Schaefer, H. F. *J. Chem. Phys.* **1986**, 84, 2262.
- Yamaguchi, Y.; Osamura, Y.; Schaefer, H. F. *J. Am. Chem. Soc.* **1983**, 105, 7506–7511.
- PSI 2.0.8. Janssen, C. L.; Seidl, E. T.; Scuseria, G. E.; Hamilton, T. P.; Yamaguchi, Y.; Remington, R. B.; Xie, Y.; Vacek, G.; Sherrill, C. D.; Crawford, T. D.; Fermann, J. T.; Allen, W. D.; Brooks, B. R.; Fitzgerald, G. B.; Fox, D. J.; Gaw, J. F.; Handy, N. C.; Laidig, W. D.; Lee, T. J.; Pitzer, R. M.; Rice, J. E.; Saxe, P.; Scheiner, A. C.; Schaefer, H. F. PSITECH, Inc.: Watkinsville, GA, 1995. This program is generally available without charge via the internet.
- Walsh, A. D. *J. Chem. Soc.* **1953**, 2260.
- Badger, R. M. *J. Chem. Phys.* **1934**, 2, 128.
- Badger, R. M. *J. Chem. Phys.* **1935**, 3, 710.
- Yamaguchi, Y.; Schaefer, H. F. *J. Chem. Phys.* **1997**, 106 (5), 1819.
- Stephens, J.; Yamaguchi, Y.; Sherrill, C. D.; Schaefer, H. F. *J. Phys. Chem.* **1998**, 102 (22), 3999.